

DOI: 10.1070/QEL16154

Post-filamentation propagation of high-power laser pulses in air in the regime of narrowly focused light channels

Yu.E. Geints, A.A. Zemlyanov, A.A. Ionin, D.V. Mokrousova,
L.V. Seleznev, D.V. Sinitsyn, E.S. Sunchugasheva

Abstract. **We report the results of experimental and theoretical studies of the post-filamentation stage of nonlinear propagation of high-power pulsed radiation from a Ti : sapphire laser in air. We have for the first time obtained the experimental dependences of the angular divergence of specific spatially localised high-intensity light structures that are observed in the beam after its multiple filamentation (post-filamentation of channels) when varying the initial focusing of laser radiation and its energy. It is found that the angular divergence of the post-filamentation channels decreases with increasing pulse energy and reducing beam numerical aperture. The experimental dependences are qualitatively interpreted based on the diffraction model of the Bessel–Gaussian beam.**

Keywords: *ultrashort laser radiation, self-focusing, filamentation, post-filament channelling.*

1. Introduction

Filamentation represents the most interesting regime of propagation of high-power laser radiation in a medium with optical nonlinearity of self-focusing (Kerr) type [1–3]. In the process of filamentation, the radiation beam disintegrates into finer threads, i.e. filaments, which possess an increased intensity and are characterised by a stable transverse size at a rather long distance. In the air and other transparent media (water, dielectrics), the peak intensity in the filament can reach tens of TW cm^{-2}, whereas the average size of a filament lies in the range from a few to hundreds micrometres, depending on the type of the propagation medium and the radiation wavelength [1]. High radiation intensity in the filaments causes ionisation of the medium molecules and leads to emergence of the concomitant plasma regions with a characteristic concentration of free electrons of 10^{15}–10^{18} cm^{-3} [4], which, in particular, are responsible for the glow of the medium in the beam channel within the visible wavelength range [5].

Yu.E. Geints, A.A. Zemlyanov V.E. Zuev Institute of Atmospheric Optics, Siberian Branch, Russian Academy of Sciences, pl. Akad. Zueva 1, 634021 Tomsk, Russia; e-mail: ygeints@iao.ru;
A.A. Ionin, L.V. Seleznev, D.V. Sinitsyn P.N. Lebedev Physics Institute, Russian Academy of Sciences, Leninsky prosp. 53, 119991 Moscow, Russia;
D.V. Mokrousova, E.S. Sunchugasheva P.N. Lebedev Physics Institute, Russian Academy of Sciences, Leninsky prosp. 53, 119991 Moscow, Russia; Moscow Institute of Physics and Technology (State University), Institutskiy per. 9, 141700 Dolgoprudnyi, Moscow region, Russia

Received 9 June 2016; revision received 30 September 2016
Kvantovaya Elektronika **46** (11) 1009–1014 (2016)
Translated by M.A. Monastyrskiy

The area of practical use of the filamentation phenomenon is quite wide and presently embraces the laser technology issues, such as femtosecond microstructuring of various media, generation of ultra-wideband radiation [6–8] and also the atmospheric-optical applications related to terrestrial electricity, remote environmental diagnostics and directional transmission of laser energy [9–12].

At the same time, as it was first established experimentally in [13], after the cessation of radiation filamentation and plasma formation, certain spatially localised light structures continue to exist in the medium within the laser beam, possessing a fairly high (several TW cm^{-2}) intensity and an abnormally low angular divergence compared to the main beam. The authors of [13] called this phenomenon the new regime of inertialess self-channelling of radiation. The first physical explanation for this effect has been proposed in [14] on the basis of the representations on self-filtration of spatial modes of the laser beam in the process of its filamentation with subsequent dominance of a weakly divergent fundamental mode on the post-filamentation phase of evolution.

Afterwards, a number of investigations have been conducted [15–18], dedicated to the study of characteristics of post-filamentation channelling and physical mechanisms responsible for their existence. In particular, Daigle et al. [15] presented experimental data on the divergence angle of the most intense central region of the light beam after its filamentation in the air. According to the estimations of the authors of this work, the divergence of the 'post-filamentation' beam, which, in accordance with [17], we hereafter for definiteness call the post-filamentation channel (PFC), amounts to about 0.03 mrad, turns out by almost an order of magnitude smaller than the divergence of the beam as a whole. In this work, a physical PFC model has been presented as a specific light structure formed after filamentation disintegration as a result of diffraction of the optical pulse field on the plasmoid formed by that pulse, and is supported by the continuing focusing action of the Kerr nonlinearity on the high-intensity beam areas.

The key role of energy periphery (energy 'reservoir') in maintaining the PFC directivity was observed in [16, 17] and indirectly confirmed by the diaphragming of the intense axial part of the beam at the stage of its post-filamentation propagation [17]. A somewhat different physical picture of the inertialess channelling of radiation was proposed in [18]: post-filamentation was considered as a result of the cubic (Kerr) self-focusing of the light channel, balanced by the defocusing effect of higher nonlinearities.

Note that the interest in the regime of inertialess self-channelling of the beam is not accidental and, apart from the scientific component, is stipulated by the possible prospects of

the practical use of intense highly directional radiation at kilometre-long distances in the atmosphere, leading to a significant expansion of the 'working area' of modern high-power femtosecond lasers [19].

In this regard, it is important to know how the spatial characteristics of the PFC depend on the initial parameters of laser radiation, in particular on its energy and focusing. To date, to our knowledge, there is no such data in the literature. In our work, we give a partial answer to this question and present the results of laboratory and numerical experiments on studying the angular divergence of high-intensity light channels formed at the stage of the post-filamentation propagation of focused femtosecond pulses from a Ti:sapphire laser with different energy in the air. It turned out that, with increasing initial energy (power) of pulses by about an order of magnitude, the angular divergence of the PFC is reduced by several times. A similar trend was observed when reducing the numerical aperture of the beam. We believe that the physical causes of the observed regularities of the post-filamentation channelling of radiation are in the combined effect of Kerr self-focusing of the field inside the high-intensity channel and the diffraction retention of the low-intensity annular areas surrounding the channel, which are formed in the process of the light beam filamentation.

2. Results and discussion

The experiments were performed with the laser pulses generated by a Ti:sapphire laser system. The FWHM pulse duration was 100 fs, the centre wavelength was 740 nm and the pulse repetition rate was 10 Hz. After exiting the laser system, the laser pulse energy was changed by the binary diffractive attenuator, after which, using a flat mirror, the pulses were directed to a focusing spherical mirror. In the experiments, we used the mirrors with the focal length f in the range from 18 to 295 cm, which corresponds to the numerical aperture NA from 0.013 to 8×10^{-4}. In accordance with the technique described in [20], we measured the longitudinal profile of linear concentration ρ_e of free electrons in the plasma produced by a laser beam in the process of filamentation.

The characteristic profile ρ_e obtained in focusing by means of a mirror with $f = 52$ cm is shown in Fig. 1. In this experiment, plasma emerged at a distance of ~15 cm from the linear focus of the beam (the focal plane in the figure corresponds to point $z = 0$). At a distance of few centimetres from the focus, the plasma concentration decreased sharply. At some distance behind the linear focus, a system for recording the transverse distribution of the laser beam energy density was placed, consisting of a screen and a lens to project the screen

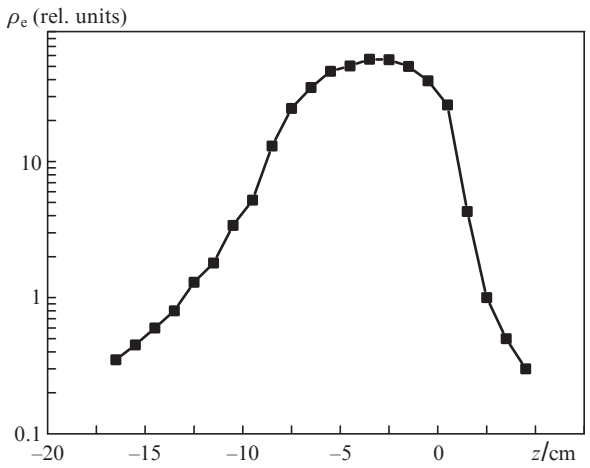

Figure 1. Longitudinal profile of the linear concentration ρ_e of plasma electrons; $f = 52$ cm, $E_0 = 3.9$ mJ.

image onto the CCD array. Moving this system along the beam axis allowed obtaining the transverse profiles of the laser beam at different distances from the linear focus.

As an example, Figs 2a and 2b show the transverse profiles of the laser beam with an initial radius $R_0 = 2.3$ mm, which is focused in the air by a mirror with $f = 52$ cm (NA = 4×10^{-3}) at various distances from the linear focus. The initial energy E_0 of the radiation pulse was 3.9 mJ, which corresponds to an approximately tenfold excess of the pulse peak power P above the critical self-focusing power $P_{cr} = 3$ GW at this wavelength. The size of each image is 16×12 mm.

It is seen that the external beam size grows with increasing distance from the focus, and the spatial separation of 'hot zones' becomes more distinct. At a distance $z = 125$ cm (Fig. 2a) four such zones, i.e. PFCs with an approximately similar transverse cross section, can be distinctly distinguished in the beam structure. Further propagation of the beam ($z = 230$ cm, Fig. 2b) leads to a decrease in the PFC energy density. The channels are located inside the beam which has rather sharply defined borders, and are surrounded by several rings emerging as a result of successive re-focusing of the pulse in the filamentation zone.

To obtain quantitative information about the PFC angular divergence, a detailed analysis of the transverse energy profiles was conducted by means of the software module we had elaborated. The result of this analysis is presented in Fig. 2 in the form of the root mean square (effective) radius of the entire beam R_b and the PFC radius r_c averaged over all allocated channels as a function of the distance.

Figure 2. Transverse profile distributions of the radiation energy density with $E_0 = 3.9$ mJ at the distances from the linear beam focus z = (a) 125 and (b) 230 cm at $f = 52$ cm; (c) dependence of the effective radius of (*1*) the entire beam R_b and (*2*) PFC r_c on the distance z from the linear focus.

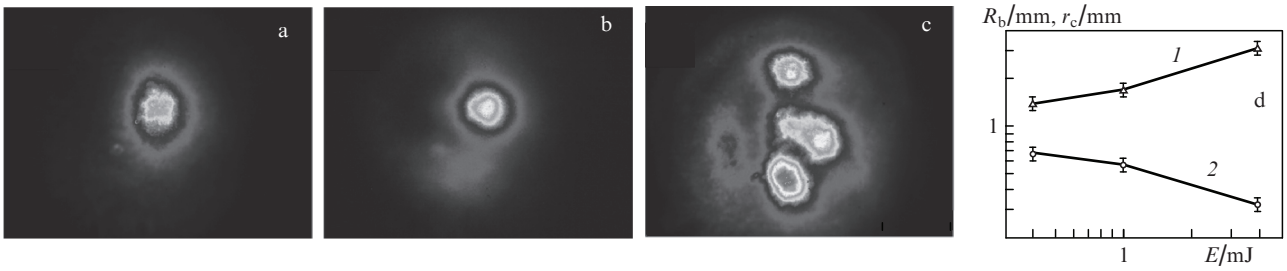

Figure 3. Transverse profile distribution of the radiation energy density with $f = 110$ cm at a distance $z = 385$ cm from the focus at $E_0 =$ (a) 0.4, (b) 1.0 and (c) 3.9 mJ; (d) dependences of the effective radius of (*1*) the entire beam R_b and (*2*) PFC r_c on the pulse energy E.

A few issues are worth of special attention. Firstly, the size of the entire beam and the radius of channels increase with increasing distance from the beam focus. Secondly, quite apparent is the fact noted in [13–18] that the PFC divergence is considerably reduced compared to the total beam divergence (difference in tilt angles). And finally, the dependence of the channel radius on the distance is almost linear. The latter allows us to represent the dependence $r_c(z)$ as a linear function: $r_c(z) = r_{c0} + \gamma_c z$, where r_{c0} is a certain initial radius of the PFC, and γ_c is the angular divergence. Thus, for the case shown in Fig. 2, this parameter is about 0.07 mrad, while the whole beam divergence behind the filamentation area is almost thirty times higher: $\gamma_b = 1.8$ mrad.

Consider the effect of initial power of the laser pulse on the spatial evolution of the emerging PFC. The laser beam transverse profile measured at the same distance from the linear focus of the mirror with $f = 110$ cm is shown in Figs 3a–3c. Each of these images is obtained at different pulse energies. It is seen that, with increasing radiation energy, firstly, the laser beam's outer size in the measurement plane increases, i.e. the beam divergence as a whole increases. Secondly, the PFC formed in the beam becomes more compact, and its intensity grows. Furthermore, there are three such channels at the maximum pulse energy (3.9 mJ). The sizes of the beam and PFC as a function of the parameter E_0 are shown in Fig. 3d.

Figure 4 shows the dependences of the angular divergence of the channels (γ_c) and the entire beam (γ_b) on the radiation energy. For convenience, all the values are normalised to the beam divergence parameter with the subcritical power $E_0 =$ 0.1 mJ, which actually corresponds to the focused radiation divergence in vacuum: $\gamma_0 = \gamma_d \sqrt{(M^2)^2 + (L_d/f)^2}$, where M^2 is the beam quality parameter; γ_d is the angular divergence; and L_d is the diffraction length of the collimated Gaussian beam.

The main conclusion that can be drawn from the data presented in Figs 3 and 4 is diametrically opposite behaviour of the beam and PFC divergences when changing the pulse energy: γ_b increases with increasing E_0, while γ_c, on the contrary, decreases. As for the growing divergence of the entire beam behind the filamentation zone with increasing beam power (energy), as is shown in [21], this is caused by the aberrations of the initially smooth radiation profile, which are a consequence of emerging ring structures surrounding the individual filaments. The higher the pulse power, the greater the number of the rings formed, and the greater the final divergence of such a distorted beam as a whole.

The trend turns out opposite [15] for post-filamentation channels, their divergence being always lower than the radiation divergence in the case of linear distribution. The reason for this, as already noted, is cubic optical nonlinearity of air,

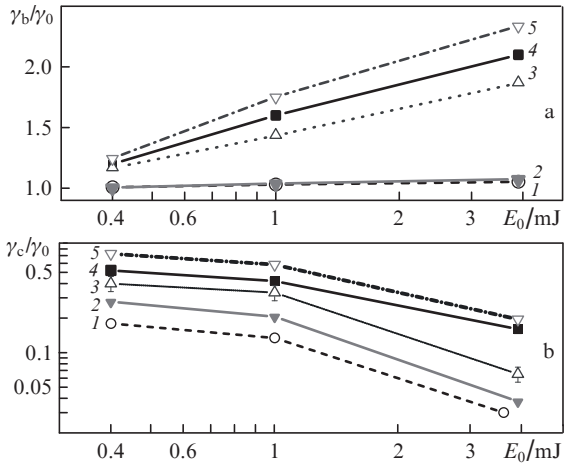

Figure 4. Experimental dependences of the normalised angular divergences of (a) the entire beam γ_b and (b) PFC γ_c on the initial pulse energy at $f =$ (*1*) 18, (*2*) 25, (*3*) 52, (*4*) 108 and (*5*) 295 cm.

the effect of which is most effective at those beam regions where the intensity is higher, i.e. within the PFC zone. Indeed, a simple numerical experiment with the Kerr effect in the programme code having been 'switched off' immediately after the pulse filamentation termination leads to equalising of γ_b and γ_c divergences.

However, the tendency for decreasing the divergence of channels with increasing E_0, which is observed in Fig. 4, can be hardly explained by the Kerr effect alone, since the intensity in the filaments that actually give start to the PFC is limited in amplitude [1] and has approximately one and the same value at any radiation power. Obviously, the reason for energy dependence in the divergence of channels must be sought for in the transverse beam profile, which, in the post-filamentation area, is different for the pulses of different power. This is well seen from Fig. 5, which shows the density distribution of the radiation energy w along one of the transverse axes, calculated for two cases with different pulse powers. The radiation is focused at a distance of 25 cm, and the profiles are constructed for $z = 45$ cm. The values of w are normalised to their maxima w_{max}, which in each case are different.

It follows from Fig. 5 that the spatial profile of the beam energy density represents a central peak surrounded by a system of rings that are formed as a result of interference of the fields at the beam periphery and filamentation zones in the course of successive refocusing of the pulse [22, 23]. It is seen that, at the same propagation distance, the low-power pulse forms the central peak with a larger cross section and a lesser

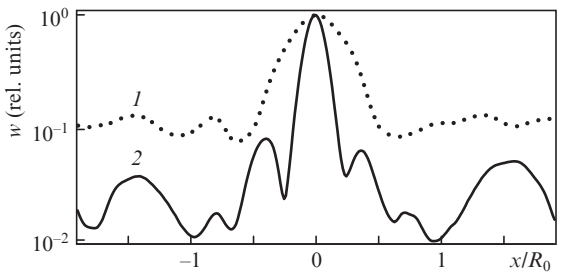

Figure 5. Transverse profile of the normalised pulse energy density at P_0/P_{cr} = (*1*) 2 and (*2*) 10.

number of surrounding rings compared to the pulse having a power that exceeds tenfold the critical one.

A good approximation to such a distribution is the Bessel–Gauss (BG) beam profile [24] which is characterised by the fact that its diffraction 'starts' not from the central intensity peak as in the Gaussian beam, but from the periphery. The BG beam has two characteristic spatial scales: the radius of its axial, most intense part (inner dimension), and the radius of the beam as a whole, including the rings (external dimension). These sizes are increased during free BG diffraction of the beam, but at different speeds.

In the framework of the BG beam diffraction model, an increase in the number of external rings around the central peak, as shown in Fig. 5b, changes the beam divergence, thus increasing the growth rate of its outer radius and simultaneously reducing the rate of broadening of its internal part. To a certain extent it simulates the situation with PFC divergence (Fig. 4b), given the known fact of increasing the number of rings in the energy density distribution around the filament with increasing pulse energy [22]. Therefore, it can be argued that the presence of a system of external rings performing the diffraction retention of a high-intensity part of the beam is necessary in order to maintain the channelled propagation of radiation at the post-filamentary stage.

For experimental verification of this hypothesis, one of the light channels formed after filamentation was cut from the laser beam by means of a circular aperture, and then a change in its size along the propagation distance was recorded. The aperture diameter and its position were chosen to guarantee the cutting-out of a ring structure around the PFC. The comparative results on the dynamics of the isolated PFC and the same channel as a part of the beam (without a diaphragm) are shown in Fig. 6 in the form of a dependence of the total channel size D_c, which is defined by the level of 0.1 in the transverse density distribution of light energy, on the distance counted from the aperture with a diameter of 1.6 mm, placed behind the focal waist at a distance z_D = 35 cm. As follows from Fig. 6, the removal of the peripheral ring structure from the PFC increases its angular divergence almost by half.

It should be noted that the data on PFC angular divergence presented in Fig. 4 were obtained in the laser pulse energy range of 0.4 mJ < E_0 < 4 mJ. A further decrease in the PFC divergence should be expected for the pulses with greater energy. However, the pace of this trend will apparently decline, and primarily due to an increase in the total number of channels formed in the post-filamentation area of propagation. This would inevitably lead to an increase in the diffraction interaction of both the PFCs themselves and the surrounding ring structures. This issue, however, requires a separate consideration.

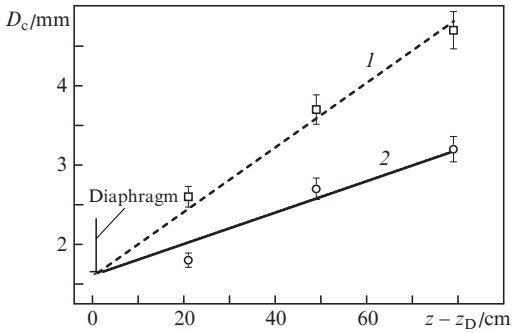

Figure 6. Dependences of the diameters of the isolated PFC (*1*) and of the same channel as a part of the beam (*2*) on the distance at E_0 = 1.4 mJ and f = 52 cm.

Figure 7 shows the PFC angular divergence and threshold of multiple channelling as functions of the numerical aperture NA of the focused beam. It can be seen that, apart from the dependence of angular divergence on the pulse energy, a quite definite dependence on the beam focusing is also observed. An increase in the numerical aperture of focusing leads to better PFC localisation relative to the entire beam. Thus, for the largest value of the numerical aperture (NA = 0.013), the ratio of the beam and channel divergences, γ_b/γ_c, depending on the initial pulse energy, lies in the range from three to thirty. At the same time, in the case of the most soft focusing, this ratio changes from approximately two to ten. However, the absolute values of the PFC divergence are increased with increasing NA (Fig. 7a) for all the radiation energies in question. This indicates that the PFC divergence is not an invariant and depends of the degree of beam focusing.

It is of interest that a change in the numerical aperture of focusing results in a change of the number of channels that are observed in the far field. At a relatively tight focusing (NA > 0.004), even a two-fold excess of the pulse power above the critical value inside the beam leads to the formation of

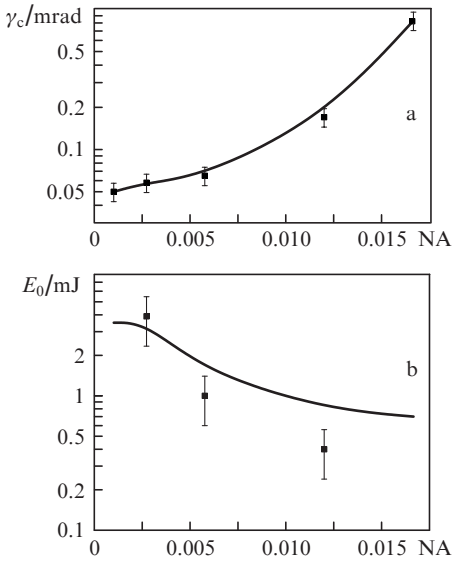

Figure 7. Dependences of the angular divergence of (a) the PFC at E_0 = 3.9 mJ and (b) the multiple filamentation threshold on the numerical aperture NA of the focused beam; points shows the experiment, solid curves represent the numerical simulation.

two or more PFCs, which indicates the presence of several filaments in the focusing area. By contrast, in the conditions of weakly focused radiation, even for a pulse, the power of which exceeds by ten times the critical value, only one intense channel is observed in the density distribution of light energy. This suggests that in this case either a certain 'threshold' of multiple filamentation (MF) of the beam was not overcome, or the MF was present; however, the channels formed from the filaments possessed a significantly different intensity, and only one of them was distinctly recorded in the observation zone. A rather large scatter in the data here is due to the fact that the pulse energy in the experiments was changed in a step-like manner, and therefore it was impossible to accurately determine the 'threshold' desired.

To study this issue, a series of numerical calculations of the MF process in the case of focused laser radiation in the air have been conducted in accordance with the technique thoroughly described in our paper [25]. In numerical experiments, an equation of quasi-optics for the complex envelope of electric field strength of a light wave with regard to the medium nonlinearity (nonlinear Schrödinger equation) was solved. The model of optical nonlinearity for the air includes the instantaneous and inertial components of the Kerr effect, nonlinearity of higher orders (saturation by the Kerr nonlinearity), a change in the complex refractive index of the medium due to photoionisation of the air molecules and the formation of a gas of free electrons. The linear part of this equation describes the group velocity dispersion of a laser pulse and the beam diffraction in the frame of phenomenological evaluation of the nonparaxial nature of the focused beam propagation [26]. To calculate the dynamics of the free electron concentration ρ_e in the beam channel, we have used the appropriate rate equation that takes into account the combined (multiphoton/tunnel) ionisation mechanism of atoms of the gas components in the atmospheric air (nitrogen, oxygen). The results of the numerical simulation for the initial laser radiation parameters that correspond to experiments are shown in Fig. 7 by the solid curves and show good agreement with experimental data.

The main causes of MF in the atmospheric-pressure air at relatively short (metre-long) tracks are associated with nonideality (non-unimodality) of the transverse amplitude–phase profile of the laser beam field at the output of the radiation shaping system. The MF itself is developed as a result of the amplitude or phase inhomogeneities if these inhomogeneities are capable of transmitting the power higher than P_{cr} [27]. Therefore, if the beam power amounts to the order of several critical values, a few filaments may, in principle, emerge.

In our experiments, the laser beam profile, though possessed an elliptical cross section, was sufficiently close to unimodal and characterised by a good quality parameter ($M^2 \sim 2$). This determined the prevailing self-focusing development of the main central maximum of the beam intensity and the dominance of this maximum on the post-filamentation stage. Calculations show that, for a weakly focusing radiation, for example, as shown in Fig. 8, with $f = 295$ cm (NA = 8×10^{-4}), multiple filaments in the focal region can be simultaneously formed even at the pulse power $P_0 > 5P_{cr}$ (the procedure of counting the number n_f of filaments is described in detail in [28]). Herewith, however, only one of them remains by the end of the filamentation zone. It is this filament that evolves into a single PFC.

If we turn now to the case of tight radiation focusing shown in Fig. 8b, the filamentation process ends here at the

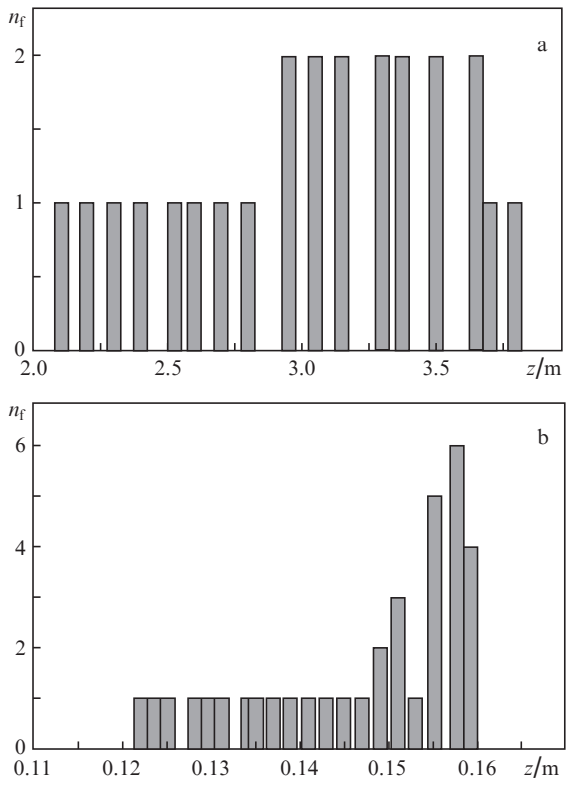

Figure 8. Number n_f of filaments formed along the laser pulse propagation distance with $P_0 = 5P_{cr}$ at f = (a) 295 and (b) 15 cm (NA = 8×10^{-4} and 0.015, respectively).

number of filaments equal to four, and just these four bright PFCs are visible on the beam energy density profiles (see Fig. 2b).

This suggests that the initially low beam divergence of a weakly focused beam facilitates active interaction (competitions [29]) of individual filaments in the focal waist, so that, as a rule, only the most intense paraxial filaments remain. In the case of tight focusing of radiation, due to abrupt reduction of the filamentation region, individual filaments have no time to noticeably influence each other. This leads to the appearance of isolated inertialess light channels in the transverse beam profile at the stage of post-filamentation propagation.

3. Conclusions

The paper discusses the post-filamentation evolution of high-power IR laser radiation in the process of its self-focusing in the air. The main attention is concentrated on the characteristics of intense spatially localised light structures formed inside the beam after the termination of filamentation, the so-called post-filamentation channels. For the first time, experimental data on the dependence of the angular divergence and the number of intense post-filamentation channels on the pulse energy and the degree of its focusing are presented.

The results of these studies confirm the existing physical model [13–15] of inertialess channelling of high-power laser radiation at the stage of its post-filamentation propagation, when high directivity of the most intense part of the beam (PFC) is ensured by the focusable Kerr nonlinearity of the medium and simultaneously is diffractively supported by a specific spatial energy distribution of the beam in the form of a system of concentric rings surrounding the channels. It is

found that the PFCs demonstrate a near-linear increase in their size with distance, while their angular divergence decreases with increasing focal length of the system and pulse energy. In the framework of the diffraction model for the Bessel–Gaussian beam, this fact can be qualitatively explained by an increase in the number of outer rings that preserve the 'diffraction-free' distribution of its axial part. The minimum divergence value of the post-filamentation channels recorded in these experiments is ~0.05 mrad at the most soft beam focusing ($f = 295$ cm) and a pulse power being tenfold greater than the critical self-focusing power in the air.

Acknowledgements. This work was supported by the Russian Science Foundation (Agreement Nos 15-17-10001 and 16-17-10128) and by the scholarship programme of the Educational and Scientific Complex, Lebedev Physics Institute, Russian Academy of Sciences.

References

1. Shen Y.R., Boyd R.W., Lukishova S.G. (Eds). *Self-focusing: Past and Present* (New York: Springer, 2009).
2. Houard A., Liu Y., Mysyrowicz A. *J. Phys.: Conf. Ser*., **497**, 012001 (2014).
3. Chekalin S.V., Kandidov V.P. *Usp. Fiz. Nauk*, **183**, 133 (2013).
4. Tzortzakis S., Prade B., Franco M., Mysyrowicz A., *Opt. Commun*., **181**, 123 (2000).
5. Ilyin A.A., Golik S.S., Shmirko K.A. *Spectrochim. Acta Part B*, **112**, 16 (2015).
6. Couairon A., Chakraborty H.S., Gaarde M.B. *Phys. Rev. A*, **77**, 053814 (2008).
7. Kiselev D., Woeste L., Wolf J.-P. *Appl. Phys. B*, **100**, 515 (2010).
8. Ionin A.A., Kudryashov S.I., Mikhin K.E., Seleznev L.V., Sinitsyn D.V. *Laser Phys*., **20**, 1778 (2010).
9. Woste L., Wedekind C., Wille H., Rairoux P., Stein B., Nikolov S., Werner Ch., Niedermeier S., Schillinger H., Sauerbrey R. *Laser Optoelektron*., **29**, 51 (1997).
10. Rodriguez M., Bourayou R., Méjean G., Kasparian J., Yu J., Salmon E., Scholz A., Stecklum B., Eislöffel J., Laux U., Hatzes A.P., Sauerbrey R., Wöste L., Wolf J.-P. *Phys. Rev. E*, **69**, 036607 (2004).
11. Ackermann R., Méchain G., Méjean G., Bourayou R., Rodriguez M., Stelmaszczyk K., Kasparian J., Yu J., Salmon E., Tzortzakis S., André Y.-B., Bourrillon J.-F., Tamin L., Cascelli J.-P., Campo C., Davoise C., Mysyrowicz A., Sauerbrey R., Wöste L., Wolf J.-P. *Appl. Phys. B.*, **82**, 561 (2006).
12. Durand M., Houard A., Prade B., Mysyrowicz A., Durécu A., Moreau B., Fleury D., Vasseur O., Borchert H., Diener K., Schmitt R., Théberge F., Chateauneuf M., Daigle J.-F., Dubois J. *Opt. Express*, **21**, 26836 (2013).
13. Méchain G., Couairon A., André Y.-B., D'Amico C., Franco M., Prade B., Tzortzakis S., Mysyrowicz A., Sauerbrey R. *Appl. Phys. B*, **79**, 379 (2004).
14. Chen Y., Théberge F., Kosareva O., Panov N., Kandidov V.P., Chin S.L. *Opt. Lett.*, **32**, 3477 (2007).
15. Daigle J.-F., Kosareva O., Panov N., Wang T.-J., Hosseini S., Yuan S., Roy G., Chin S.L. *Opt. Commun*. **284**, 3601 (2011).
16. Daigle J.-F., Wang T.-J., Hosseini S., Yuan S., Roy G., Chin S.L. *Appl. Opt*., **50**, 6234 (2011).
17. Gao H., Liu W., Chin S.L. *Laser Phys.*, **24**, 055301 (2014).
18. Zheltikov A., Mitrofanov A., Voronin A., Sidorov-Biryukov D., Fedotov A., Baltuska A., Pugzlys A., Flöry T., Andriukaitis G., Panchenko V., Mikhailova J. *Opt. Lett*., **39**, 4659 (2014).
19. Durand M., Houard A., Prade B., Mysyrowicz A., Durécu A., Moreau B., Fleury D., Vasseur O., Borchert H., Diener K., Schmitt R., Théberge F., Chateauneuf M., Daigle J.F., Dubois J. *Opt. Express*, **21**, 26836 (2013).
20. Geints Yu.E., Zemlyanov A.A., Ionin A.A., Mokrousova D.V., Seleznev L.V., Sinitsyn D.V., Sunchugasheva E.S. *Kvantovaya Elektron*., **45**, 321 (2015) [*Quantum Electron*., **45**, 321 (2015)].
21. Zemlyanov A.A., Bulygin A.D., Geints Yu.E. *Opt. Atmos. Okeana*, **26**, 350 (2013).
22. Chin S.L., Akozbek N., Proulx A., Petit S., Bowden C.M. *Opt. Commun*., **188**, 181 (2001).
23. Zemlyanov A.A., Geints Y.E. *EPJ D*, **42**, 349 (2006).
24. Gori F., Guattari G., Padovani C. *Opt. Commun.*, **64**, 491 (1987).
25. Geints Yu.E., Golik S.S., Zemlyanov A.A., Kabanov A.M., Matvienko G.G. *Kvantovaya Elektron*., **44**, 489 (2014) [*Quantum Electron*., **44**, 489 (2014)].
26. Geints Yu.E., Zemlyanov A.A., Kabanov A.M., Matvienko G.G., Stepanov A.N. *Opt. Atmos. Okeana*, **25**, 745 (2012).
27. Bespalov V.I., Talanov V.I. *Pis'ma Zh. Eksp. Teor. Fiz*., **3**, 471 (1966).
28. Geints Yu.E., Golik S.S., Zemlyanov A.A., Kabanov A.M., Petrov A.V. *Kvantovaya Elektron*., **46**, 133 (2016) [*Quantum Electron*., **46**, 133 (2016)].
29. Chin S.L., Petit S., Liu W., Iwasaki A., Nadeau M.-C., Kandidov V.P., Kosareva O.G., Andrianov K.Yu. *Opt. Commun*., **210**, 329 (2002).